Gravity-driven enhancement of heavy particle clustering in turbulent flow

Jérémie Bec,[1] Holger Homann,[1] and Samriddhi Sankar Ray[2]

[1] *Laboratoire Lagrange, Université de Nice-Sophia Antipolis, CNRS, OCA, Bd. de l'Observatoire, 06300 Nice, France*
[2] *International Centre for Theoretical Sciences, Tata Institute of Fundamental Research, Bangalore 560012, India*

Heavy particles suspended in a turbulent flow settle faster than in a still fluid. This effect stems from a preferential sampling of the regions where the fluid flows downward and is quantified here as a function of the level of turbulence, of particle inertia, and of the ratio between gravity and turbulent accelerations. By using analytical methods and detailed, state-of-the-art numerical simulations, settling is shown to induce an effective horizontal two-dimensional dynamics that increases clustering and reduce relative velocities between particles. These two competing effects can either increase or decrease the geometrical collision rates between same-size particles and are crucial for realistic modeling of coalescing particles.

arXiv:1401.1306v1 [physics.flu-dyn] 7 Jan 2014

Many industrial, atmospheric, and astrophysical phenomena ranging from the microphysics of cloud formation, to planet formation in a dusty circumstellar disk of gas, involves the modeling of the interactions between small solid particles suspended in a turbulent carrier flow. Two main effects are typically at play: a viscous drag that particles experience with the agitated fluid and an external force, such as gravity, that acts because of their density contrast with the fluid. While drag is predominant for small particles, gravity takes over the dynamics of large particles and most studies treat these two asymptotics independently. However it is usually at this critical transition that standard modeling fails, as is evident when estimating for instance the rate at which rain is triggered in warm clouds [1, 2]. Most models are unable to circumvent a bottleneck in the droplet growth for diameters around 20-40μm. A key improvement might be to combine turbulent and gravitational effects.

In this Letter we understand the intriguing interplay between turbulence, gravity, and particle sizes. This question is of fundamental importance in fluid dynamics, in particular, and in non-equilibrium statistical physics, in general, as it is central to modeling coalescences in natural or laboratory droplet suspensions. The most noticeable effect of turbulence on the settling of heavy particles is the increase of their terminal velocity induced by a preferential sweeping along the downward fluid flow [3–5]. This phenomenon is mostly understood on qualitative grounds and has been quantified only in model flows [6]. Furthermore very little is known on the effect of gravitational settling on two-particle statistics. Fundamental theoretical and numerical studies of the clustering of particle pairs [7, 8] and of the enhancement of collisions due to inertia [9, 10] usually neglect gravity. We present here, by combining state-of-the-art direct numerical simulations with theoretical results based on our asymptotic analysis, a systematic study of the dynamical and statistical properties of particles as a function of *(i)* the level of turbulence of the carrier flow (Reynolds number), *(ii)* the inertia of the particles (Stokes number), and *(iii)* the ratio between the turbulent accelerations and gravity (Froude number).

We consider a fluid flow whose velocity $\boldsymbol{u}$ is a solution to the incompressible Navier–Stokes equation

$$\partial_t \boldsymbol{u} + (\boldsymbol{u}\cdot\nabla)\boldsymbol{u} = -\nabla p + \nu\nabla^2\boldsymbol{u} + \boldsymbol{f}, \quad \nabla\cdot\boldsymbol{u} = 0, \quad (1)$$

where ν is the fluid kinematic viscosity. Homogeneous isotropic turbulence is maintained in a statistical steady state by the large-scale forcing $\boldsymbol{f}$. We perform direct numerical simulations by using the parallel solver *LaTu*, which is pseudo-spectral in space and involves a third-order Runge–Kutta scheme for time marching. We use different spatial resolutions, 256^3, 1024^3, and 2048^3 corresponding to Taylor-scale Reynolds numbers $R_\lambda = u_{\rm rms}\sqrt{15/(\varepsilon\nu)} \approx 130$, 290, and 460, respectively ($u_{\rm rms} = \langle u_x^2\rangle$ is the root-mean-square velocity and $\varepsilon = \nu\langle\|\nabla\boldsymbol{u}\|^2\rangle$ the average dissipation rate; see [11]).

Particles are assumed much smaller than any turbulent scale, much heavier than the surrounding fluid, and with a small Reynolds number associated to their slip velocity. They are then moved by the fluid through a viscous Stokes drag and their trajectories $\boldsymbol{X}_{\rm p}(t)$ follow

$$\frac{{\rm d}\boldsymbol{X}_{\rm p}}{{\rm d}t} = \boldsymbol{V}_{\rm p}, \quad \frac{{\rm d}\boldsymbol{V}_{\rm p}}{{\rm d}t} = -\frac{1}{\tau_{\rm p}}\left[\boldsymbol{V}_{\rm p} - \boldsymbol{u}(\boldsymbol{X}_{\rm p},t)\right] + \boldsymbol{g}, \quad (2)$$

where $\boldsymbol{g}$ is the acceleration of gravity. The relaxation time reads $\tau_{\rm p} = 2\rho_{\rm p}a^2/(9\rho_{\rm f}\nu)$, $\rho_{\rm p}$ and $\rho_{\rm f}$ being the particle and fluid mass density and a the particle radius. In our simulations individual particle trajectories are integrated for different values of $\tau_{\rm p}$ and $g = |\boldsymbol{g}|$. The fluid velocity at the location of the particles is evaluated by linear interpolation. Particle inertia is measured in terms of the *Stokes number* $St = \tau_{\rm p}/\tau_\eta$ where $\tau_\eta = \sqrt{\nu/\varepsilon}$ is the turnover time associated to the Kolmogorov dissipative scale $\eta = \nu^{3/4}/\varepsilon^{1/4}$. The effect of gravity is measured by the *Froude number* $Fr = \varepsilon^{3/4}/(g\nu^{1/4})$ defined as the ratio between the typical turbulent acceleration η/τ_η^2 and that of gravity. In all our simulations we have used 10 different Stokes numbers and 5 different values of the Froude number (including the case of no gravity). Furthermore, to obtain reliable statistics, we use a very large number of particles N_p, in each of our simulations; for $R_\lambda \approx 460, N_p = 10^9$, for $R_\lambda \approx 290, N_p = 1.28\times10^8$, and $R_\lambda \approx 130, N_p = 8\times10^6$.

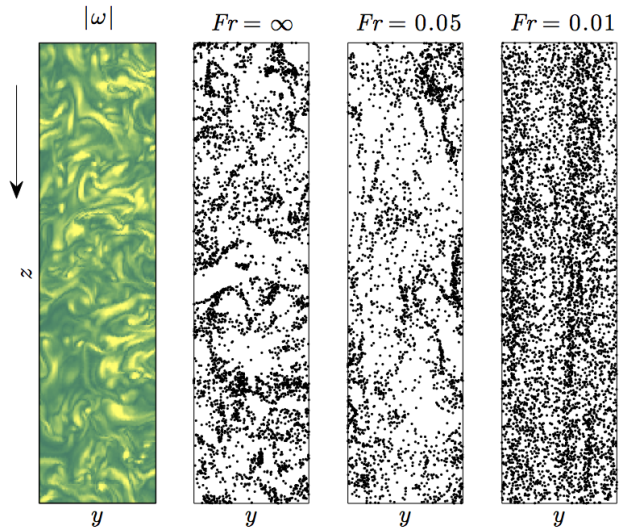


FIG. 1. (color online) Snapshot of the vorticity modulus (Left; yellow = low values, green = high values) and of the particle positions for $R_\lambda = 130$, $St = 1$ and three different values of the Froude number in a slice of thickness 10η, width 130η, and height 520η. The vertical arrow indicates gravity.

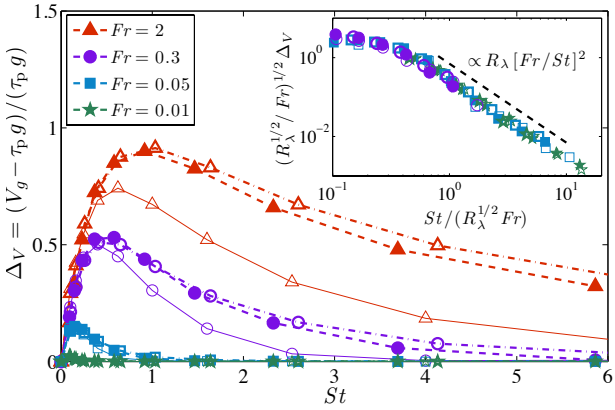


FIG. 2. (color online) Relative increase of the settling velocity Δ_V as a function of the Stokes number St for various Froude numbers, as labeled, and $R_\lambda = 130$ (thin symbols, plain lines), $R_\lambda = 290$ (filled symbols, dashed lines) and $R_\lambda = 460$ (open symbols, broken lines). Inset: $[R_\lambda^{1/2}/Fr]^{1/2}\Delta_V$ as a function of $St/[R_\lambda^{1/2} Fr]$ for the same data.

Figure 1 shows a representative snapshot of the modulus of the vorticity $\boldsymbol{\omega} = \nabla \times \boldsymbol{u}$ in a thin slice of our three-dimensional flow, together with the position of particles with the same Stokes ($St = 1$) but different Froude numbers Fr. We observe that when gravity is negligible ($Fr = \infty$), the particle distribution correlates with low-vorticity regions. Increasing the effect of gravity does not instantaneously destroy particle clusters but rather give them some anisotropy as they get more and more aligned with the vertical direction $\hat{\boldsymbol{e}}_z = -\boldsymbol{g}/g$. This indicates that settling is responsible for a two-dimensionalization of the particles dynamics and, as observed on the right-most panel, clustering is still present but concentration gradients are mainly in the horizontal directions.

To understand further the underlying mechanisms, let us estimate the average settling velocity $V_g = -\langle \boldsymbol{V}_\mathrm{p} \cdot \hat{\boldsymbol{e}}_z \rangle$. Clearly from (2), the statistical stationarity of the particle velocity implies that $V_g = \tau_\mathrm{p} g - \langle u_z(\boldsymbol{X}_\mathrm{p}, t) \rangle$. The first term is equal to the terminal velocity of a particle with response time τ_p in a still fluid. It was observed that settling particles in a turbulent flow are more likely to sample regions where the vertical fluid velocity is aligned with gravity, leading to an enhancement of their average settling speed [3, 4]. This effect is also observed in our simulations as shown in Fig. 2 which represents the relative increase in settling velocity $\Delta_V = (V_g - \tau_\mathrm{p} g)/(\tau_\mathrm{p} g) = -\langle u_z(\boldsymbol{X}_\mathrm{p}, t) \rangle/(\tau_\mathrm{p} g)$ (compared to the terminal velocity in still fluid) as a function of the particle Stokes number and for different values of Fr and R_λ. One notices that the effect is the strongest for the largest values of the Froude number (when turbulent accelerations dominate over gravity) and, at sufficiently large particle inertia. Conversely, for low-inertia particles ($St \ll 1$), the gain Δ_V is almost independent of both the Reynolds and the Froude numbers.

To understand quantitatively these observations, let us first consider the asymptotics $St \ll 1$. To leading order, the particles are as if advected by an effective compressible velocity field [3], namely $\boldsymbol{V}_\mathrm{p} \approx \boldsymbol{v}(\boldsymbol{X}_\mathrm{p}, t)$ with

$$\boldsymbol{v} = \boldsymbol{u} - \tau_\mathrm{p} \left[\partial_t \boldsymbol{u} + (\boldsymbol{u} + \tau_\mathrm{p} \boldsymbol{g}) \cdot \nabla \boldsymbol{u} \right]. \qquad (3)$$

We focus on the motion in the horizontal directions (x, y) transverse to that of gravity and use (3) to write the correlation $\langle u_z \nabla_\perp \cdot \boldsymbol{v}_\perp \rangle$, where $\boldsymbol{v}_\perp = (v_x, v_y)$. All terms except the advection due to settling vanish by incompressibility or isotropy of the fluid velocity field, so that

$$\langle u_z \nabla_\perp \cdot \boldsymbol{v}_\perp \rangle = \tau_\mathrm{p}^2 g \left\langle (\partial_z u_z)^2 \right\rangle > 0. \qquad (4)$$

Hence, the horizontal clustering of particles (negative divergence) is on average where the flow heads downward ($u_z < 0$). This quantifies the preferential sweeping ideas of [4]. With arguments similar to those used in [1] (see also [12]) for density correlations, we can relate the average vertical velocity along particle paths to the correlation (4). In the limit $St \ll 1$, the divergence $\nabla_\perp \cdot \boldsymbol{v}_\perp$ gives indeed the bias due to the preferential sampling by inertial particles. This leads to $\langle u_z(\boldsymbol{X}_\mathrm{p}, t) \rangle \propto \tau_\eta \langle u_z \nabla_\perp \cdot \boldsymbol{v}_\perp \rangle$ and by using (4) to $\Delta_V \propto \tau_\eta \tau_\mathrm{p} \left\langle (\partial_z u_z)^2 \right\rangle \propto St$, confirming the linear behavior independent of Fr and R_λ observed in Fig. 2 at small Stokes numbers.

In the other asymptotics ($St \gg 1$), the settling velocity V_g gets very large and the fluid velocity seen by the particles becomes short-correlated in time. The particles have an almost ballistic motion in the vertical direction and diffuse in the horizontal plane. This occurs when the time L/V_g, required by the particle to traverse the

integral scale $L = u_{\rm rms}^3/\varepsilon$, is much shorter than the large-scale correlation time $\tau_L = L/u_{\rm rms}$. Rescaling time by $\tau_L(V_g/u_{\rm rms})$ and space by L leads to approximating the horizontal dynamics in non-dimensional units as

$$\frac{{\rm d}\boldsymbol{V}_{\rm p}^{\perp}}{{\rm d}s} \simeq -\frac{1}{\bar{S}}\left[\boldsymbol{V}_{\rm p}^{\perp} - \tilde{\boldsymbol{u}}(\boldsymbol{X}_{\rm p}^{\perp}, s)\right] \tag{5}$$

where $\bar{S} = (\tau_{\rm p}/\tau_L)(u_{\rm rms}/V_g)$ and $\tilde{\boldsymbol{u}}$ is a two-dimensional white-noise-in-time velocity field whose correlations have the same spatial structure as $\boldsymbol{u}$. This approach is similar to that developed in [13] for particles with very large inertia. Hence, the rescaled single-particle statistical properties depend only on the effective Stokes number $\bar{S}$. In particular, the falling speed of the particle takes the form $V_g \simeq \tau_{\rm p}\, g + u_{\rm rms}^2 \Psi(\bar{S})/V_g$ where Ψ is a non-dimensional function that accounts for preferential sampling. To leading order $V_g \simeq \tau_{\rm p}\, g$, so that $\Delta_V \sim \Psi(\bar{S})\, R_\lambda\, (Fr/St)^2$ and $\bar{S} \sim Fr/\sqrt{R_\lambda} \ll 1$, which is independent of the particle Stokes number. As the velocity field appearing in (5) is a white-noise, one expects that for $\bar{S} \ll 1$ statistical observables can be written as a series of half-integer powers of $\bar{S}$ (see, *e.g.*, [14]), so that $\Psi(\bar{S}) \sim \bar{S}^{1/2}$. This leads to

$$\Delta_V \propto R_\lambda^{3/4} Fr^{5/3} St^{-2} \tag{6}$$

for $St \gg R_\lambda^{1/2} Fr$ and $Fr \ll R_\lambda^{1/2}$. This behavior is confirmed by our data, as can be seen in the inset of Fig. 2.

We now turn to small-scale two-particle statistics. The approach in terms of the effective dynamics (5) extends to the linearized dynamics, *i.e.* to the tangent system associated to (2), which describes the evolution of infinitesimal separations between particles in terms of the fluid gradient $\nabla\boldsymbol{u}$ along their paths. When the fall speed is large enough, the particles travel through the correlation length η of $\nabla\boldsymbol{u}$ in a time shorter than its correlation time τ_η. This occurs when $V_g \gg u_\eta = \eta/\tau_\eta = (\nu\varepsilon)^{1/4}$. Rescaling time by $\tau_\eta(V_g/u_\eta)$ and space by the Kolmogorov scale η allows one to approximate the time-evolution of the separation $\boldsymbol{R}$ as

$$\frac{{\rm d}^2\boldsymbol{R}}{{\rm d}s^2} \simeq -\frac{1}{\tilde{S}}\left[\frac{{\rm d}\boldsymbol{R}}{{\rm d}s} - \boldsymbol{R}\cdot\boldsymbol{\sigma}(s)\right], \tag{7}$$

where $\boldsymbol{\sigma}$ is a Gaussian tensorial noise with co-variance $\langle\sigma_{ij}(s)\sigma_{k\ell}(s')\rangle = (\nu/\varepsilon)\langle\partial_i u_j \partial_k u_\ell\rangle\delta(s-s')$. The one-point one-time strain tensor co-variance is here evaluated along particle paths to account for preferential sampling. The effective Stokes number now reads $\tilde{S} = St\,(u_\eta/V_g)$ and in the asymptotics $V_g \gg u_\eta$, small-scale two-particle statistics depend solely on $\tilde{S}$. Remarkably, when the settling velocity is close to that in still fluid (*i.e.* $\Delta_V \ll 1$), the effective Stokes reads $\tilde{S} \simeq Fr$, so that statistics become independent of St when $St \gg Fr$.

An important observable measuring particle clustering is the correlation dimension $\mathcal{D}_2$ of their spatial distribution [8]. It is given by $\mathbb{P}_2(r) \propto r^{\mathcal{D}_2}$ for $r \ll \eta$, where

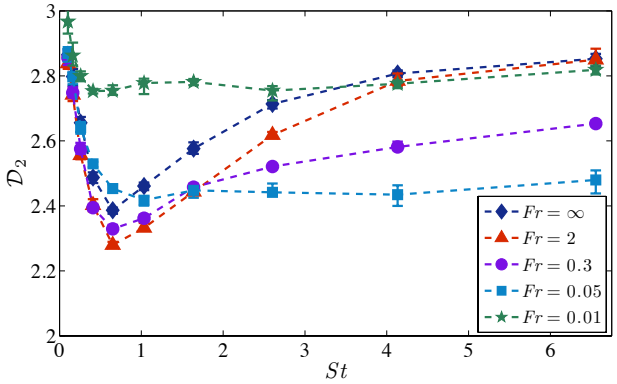


FIG. 3. (color online) Correlation dimension $\mathcal{D}_2$ of the particle distribution as a function of the Stokes number for $R_\lambda = 460$ and various Froude numbers as labeled. Smaller Reynolds numbers (not shown here) display a similar behavior.

$\mathbb{P}_2(r)$ is the probability that two particles are within a distance r. This fractal dimension is shown in Fig. 3 as a function of St for different values of Fr and $R_\lambda = 460$. One observes that gravity acts in a non-uniform manner. It tends to enhance concentration (decrease $\mathcal{D}_2$) when both the Stokes and the Froude numbers have moderate values. When $Fr \ll 1$, clustering is decreased for $St \lesssim 1$ and increased for $St \gtrsim 1$. For all finite Fr, one observes that $\mathcal{D}_2$ saturates to a finite value when $St \to \infty$. This can be explained by the equivalence between the two-points dynamics and (7). For $V_g \gg u_\eta$, the fractal dimension $\mathcal{D}_2$ is a function of the effective Stokes number $\tilde{S}$ only, which for $St \gg Fr$ becomes independent of St. In this asymptotics, the correlation dimension depends solely on Fr. The limiting value of $\mathcal{D}_2$ is a non-monotonic function of Fr. It is close to 3 when either $Fr \gg 1$ or $Fr \ll 1$ as the corresponding values of $\bar{S} \sim Fr$ characterizing the dynamics (7) are related in both cases to space-filling distributions. In delta-correlated flows, the correlation dimension is known to behave linearly at small Stokes numbers [14]. It is hence expected that for $Fr \ll 1$, $\mathcal{D}_2 \simeq 3 - C\,Fr$ where C is a positive constant.

The increase in clustering observed for order-unity values of St and Fr means that settling can significantly impact the timescales of interaction between particles. When interested for instance in the collisions, estimations of the geometrical rate involve the probability density that two particles are at a distance $r = 2a$ equal to the sum of their radii and thus scales as $(2a)^{\mathcal{D}_2-1}$. However, this quantity alone is not enough as the collision rate involves also the typical velocity at which particles approach each other. Indeed, for same-size particles, it is given by setting $r = 2a$ in the approaching rate [15]

$$\kappa(r) = -\left\langle w\,\theta(-w)\,\delta(|\boldsymbol{R}| - r)\right\rangle, \tag{8}$$

where $w = {\rm d}|\boldsymbol{R}|/{\rm d}t$ is the longitudinal velocity difference between particles, θ the Heaviside function, and $\langle\cdot\rangle$ the

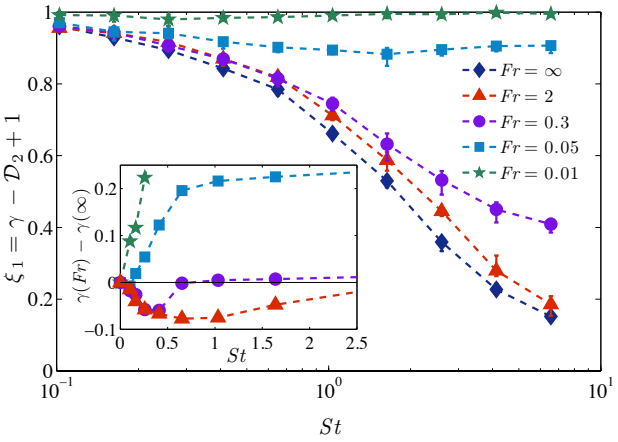


FIG. 4. (color online) Exponent of the velocity difference $\xi_1 = \gamma - \mathcal{D}_2 + 1$ as a function of the Stokes number for different Fr and $R_\lambda = 460$. Inset: difference between the approaching rate exponent γ associated to the different values of Fr and that associated to particles feeling no gravity ($Fr = \infty$). Smaller Reynolds numbers (not shown here) behave similarly.

average over all particle separations $\boldsymbol{R}$. The approaching rate can be expressed in terms of a conditional average $\kappa(r) = -\langle w\,\theta(-w)|\,|\boldsymbol{R}|=r\rangle\,(\mathrm{d}\mathbb{P}_2/\mathrm{d}r)$, which involves the average negative longitudinal velocity difference between particles separated by a distance r. This last quantity behaves also as a power of r for $r \ll \eta$ with an exponent ξ_1 given by the first-order structure function of particle velocities [10]. This implies that $\kappa(r) \sim r^\gamma$ with $\gamma = \xi_1 + \mathcal{D}_2 - 1$. The dependence of γ upon St, which encompasses particle clustering and velocity differences statistics, determines how the collision rate depends on the particles size and inertia. Figure 4 shows the velocity scaling exponent ξ_1 as a function of St for the various relative strengths of gravity we have investigated. In the case of no gravity ($Fr = \infty$), the particle velocity scaling exponent goes from a behavior close to that of tracers ($\xi_1 = 1$) at small St to an uncorrelated gas with scale-independent velocity differences ($\xi_1 = 0$) for $St \to \infty$. This transition relates to the formation of fold caustics in the particle velocity field [9, 15]. Gravity acts this time in a monotonic manner since ξ_1 systematically increases when Fr decreases, indicating that settling weakens small-scale velocity differences between particles. The underlying mechanisms can be understood in the asymptotics $St \gg Fr$, again in terms of the equivalent small-scale dynamics (7). When Fr decreases, the effective Stokes number decreases, so that particles get closer to tracers of the effective flow and $\xi_1 \to 1$.

The two mechanisms determining the rate at which particles collide, namely preferential concentration and large velocity differences, are thus affected in competing manners by gravity. However the enhancement of particle clustering takes over the decrease of velocity differences when $St \lesssim Fr$. This is evident in the inset of Fig. 4, which shows the difference of the approaching rate scaling exponents $\gamma(Fr) - \gamma(\infty)$ between particles undergoing gravity and those that do not. One clearly observes that $\gamma(Fr) < \gamma(\infty)$ for $St \lesssim Fr$, indicating that in this range collision rates between same-size particles are larger in the presence of gravity. At first glance these corrections could seem tiny. However, they are responsible for an important increase of the geometrical collision rate. For instance, in highly-turbulent cloud settings, namely $Fr = 0.3$ (corresponding to $\varepsilon \approx 1000\,cm^2/s$ for the turbulent airflow), we find an increase by more than a factor two of the collision rate between $St = 0.4$ particles (droplets with diameter $\approx 30\,\mu m$). This newly identified effect, which combines turbulence and gravitational settling, clearly needs to be borne in mind when improving existing models for coalescing particle or droplet suspensions.

This research has received funding from the European Research Council under the European Community's Seventh Framework Program (FP7/2007-2013 Grant Agreement No. 240579) and from the French Agence Nationale de la Recherche (grant BLAN07-1_192604). Access to the IBM BlueGene/P computer JUGENE at the FZ Jülich was made available through the PRACE project PRA031. JB and SSR acknowledge support from the Indo-French Centre for Applied Mathematics and SSR from the EADS Corporate Foundation Chair, awarded to ICTS-TIFR and TIFR-CAM.

[1] G. Falkovich, A. Fouxon, and M. Stepanov, Nature **419**, 151 (2002).
[2] W. Grabowski and L.-P. Wang, Ann. Rev. Fluid Mech. **45**, 293 (2013).
[3] M. Maxey, J. Fluid Mech. **174**, 441 (1987).
[4] L.-P. Wang and M. Maxey, J. Fluid Mech. **256**, 27 (1993).
[5] O. Ayala, B. Rosa, L.-P. Wang, and W. Grabowski, New J. Phys. **10**, 075015 (2008).
[6] J. Davila and J. Hunt, J. Fluid Mech. **440**, 117 (2001).
[7] E. Balkovsky, G. Falkovich, and A. Fouxon, Phys. Rev. Lett. **86**, 2790 (2001).
[8] J. Bec, L. Biferale, M. Cencini, A. Lanotte, S. Musacchio, and F. Toschi, Phys. Rev. Lett. **98**, 84502 (2007).
[9] M. Wilkinson, B. Mehlig, and V. Bezuglyy, Phys. Rev. Lett. **97**, 048501 (2006).
[10] J. Bec, L. Biferale, M. Cencini, A. Lanotte, and F. Toschi, J. Fluid Mech. **646**, 527 (2010).
[11] U. Frisch, *Turbulence* (Cambridge University Press, 1996).
[12] I. Fouxon, Phys. Rev. Lett. **108**, 134502 (2012).
[13] I. Fouxon and P. Horvai, Phys. Rev. Lett. **100**, 040601 (2008).
[14] J. Bec, M. Cencini, R. Hillerbrand, and K. Turitsyn, Physica D **237**, 2037 (2008).
[15] J. Bec, A. Celani, M. Cencini, and S. Musacchio, Phys. Fluids **17**, 073301 (2005).